Impact of Multivariate Granger Causality Analyses with Embedded Dimension Reduction on Network Modules

Christoph Schmidt[1*], Britta Pester[1*], Mahesh Nagarajan[2], Herbert Witte[1], Lutz Leistritz[1], Axel Wismueller[2]

Abstract— **High dimensional functional MRI data in combination with a low temporal resolution imposes computational limits on classical Granger Causality analyses with respect to a large-scale representations of functional interactions in the brain. To overcome these limitations and exploit information inherent in resulting brain connectivity networks at the large scale, we propose a multivariate Granger Causality approach with embedded dimension reduction. Using this approach, we computed binary connectivity networks from resting state fMRI images and analyzed them with respect to network module structure, which might be linked to distinct brain regions with an increased density of particular interaction patterns as compared to inter-module regions. As a proof of concept, we show that the modular structure of these large-scale connectivity networks can be recovered. These results are promising since further analysis of large-scale brain network partitions into modules might prove valuable for understanding and tracing changes in brain connectivity at a more detailed resolution level than before.**

I. INTRODUCTION

Granger Causality approaches are frequently applied to identify directed functional connectivity in neural time series data [1]. However, it is restricted by the dimensionality of the underlying time series. To overcome this limitation we propose a fully multivariate Granger Causality approach with embedded dimension reduction to compute highly resolved brain functional connectivity networks that can be analyzed with respect to topological segmentation. A long-term objective might be a full brain representation without any predefinition of ROIs or specific voxels. The identification and clustering of network vertices with similar coupling patterns within the network may be used for functional segmentation, which can directly be projected onto neuroimaging data. Consequently, we are interested in the tradeoff between computing increasingly higher dimensional connectivity networks and the resulting loss of topological information as shown by the quality of recovered network modules (network communities).

Recently, the large-scale Granger Causality Index (lsGCI) has been introduced as a possible means to quantify directed information transfer in very high-dimensional systems [2]. The basic idea is the insertion of a dimension reduction into model estimation, which allows computation of prediction errors in the original high-dimensional space. Here we examine the effects of this procedure on network module structure by means of several simulated time series and one exemplary resting state fMRI data set.

This study was supported by the grant 01GQ1202 of the Federal Ministry of Education and Research (Germany), as well as by the NIH grant 1R01DA034977-01 (USA).

[1]Bernstein Group for Computational Neuroscience Jena, Institute of Medical Statistics, Computer Sciences and Documentation, Jena University Hospital, Friedrich Schiller University Jena, Bachstrasse 18, 07747 Jena, Germany, [2]Department of Imaging Sciences, Department of Biomedical Engineering, University of Rochester Medical Center, Rochester, New York, USA, *Both authors contributed equally.

II. MATERIAL

A. Ground truth networks with known module structure

To test the effect of dimension reduction on network module structure and for comparing the lsGCI approach with the conventional Granger Causality Index we simulated binary directed ground truth (ad hoc) networks of size $D = 50$ with known module structure. Given a predefined number of modules and their sizes (two modules of size 12, two modules of size 13), vertices are selected and accordingly assigned membership to non-overlapping modules. The edges connecting these vertices in the ground truth networks are placed randomly under constraints that define a notion of module structure. Edge patterns are constrained by probabilities for internal edges (intra-module) and external edges (inter-module) between all vertices and also additional conditions on minimum internal and maximum external in- and out-degrees have to hold true. The probability of connections within each module was set to 0.7, the probability of connections between vertices of different modules was set to 0.02. The minimum internal in-degree of a vertex specifies the lower bound for the number of its incoming connections from member vertices of its assigned module. In our simulations this parameter and the minimum number of internal out-degrees were both set to 6. The maximum allowed external in-degree of each vertex constitutes the upper bound for the number of in-coming connections from vertices of different modules. This parameter and the maximum external out-degree were set to 4. Note that the constraints on internal and external degrees do not entail a determination of specific connection patterns between vertices. The ground truth networks are obtained by combining the adjacency matrix of a network that represents only the edges within communities with another one that represents edges between vertices of different communities (Fig. 1(a)). This splitting of the problem makes the computations involved much more tractable.

Based on the resulting adjacency matrices $\mathbf{A} \in \{0,1\}^{D\times D}$ we realized stationary first order multivariate autoregressive (MVAR) processes $\mathrm{Y}(n) = \mathbf{B} \cdot \mathrm{Y}(n-1) + \mathrm{E}(n) \in \mathbb{R}^D$, for $n = 1, \ldots, N$, with zero mean, uncorrelated Gaussian processes $\mathrm{E}(n)$. To ensure stationarity, the model parameters

978-1-4244-7929-0/14/$26.00 ©2014 IEEE

were set to $b_{ij} = 0.99 \cdot \rho \cdot a_{ji}/\eta$, where η is the maximum column sum of $\mathbf{A}$, and ρ is a uniformly distributed sign.

B. Resting state fMRI data

Functional MRI images of healthy subject were acquired with a 3.0 T Siemens MAGNETOM Trio TIM scanner (Siemens, Erlangen, Germany) with a standard birdcage head coil. Resting state (EPI-BOLD) sequences were performed with the following parameters: echo time (TE) - 30 ms, echo-repetition time (TR) - 2s, and flip angle (FA) - 90 degrees. The acquisition lasted 6 minutes and 40 seconds during which 200 volumes of functional data were acquired. Each volume consisted of 30 axial slices with an in-plane resolution of 4 mm x 4 mm. The inter-slice distance was 4mm. During the scan, the subject was instructed to stay still and keep eyes closed.

To aid in localization and registration of functional data, a high-resolution T1-weighted MPRAGE sequence was acquired with the following parameters: TE - 3.44 ms, TR - 2.53 s and FA - 7 degrees. 192 slices were acquired in the sagittal direction with an in-plane resolution of 1 mm x 1 mm and a slice thickness of 1 mm. Functional MRI data was then preprocessed using FSL v4.1.9. Data volumes were motion corrected, brain extracted, temporally filtered with a high-pass filter of cut-off frequency 0.005 Hz, and normalized to MNI152 brain atlas.

To give a proof of principle of the proposed methodology, we used one slice (slice number 10) for our analysis providing 1031 voxels associated to the brain. The MVAR model order was set to 6, which reflects a compromise between model simplicity and sufficient fit amongst FFT spectra and corresponding parametric AR spectra.

III. METHODS

A. Large scale Granger Causality Index

A D-dimensional, p-th order MVAR process is given by $\mathrm{Y}(n) = \sum_{r=1}^{p} \mathbf{B}^r \mathrm{Y}(n-r) + \mathrm{E}(n) \in \mathbb{R}^D,\ n = 1, \ldots, N$, with AR-parameters $\mathbf{B}^r \in \mathbb{R}^{D \times D}$ and a zero mean, uncorrelated noise process $\mathrm{E}(n)$. In the case of high dimensional (HD) data, a simple AR estimation is not feasible due to its computational complexity. Thus, in a first stage PCA serves as a preprocessing step for dimension reduction: $\mathbf{X} = \mathbf{W}\mathbf{Y}$, with $\mathbf{Y} = \big(\mathrm{Y}(1), \ldots, \mathrm{Y}(N)\big)$, the principal component (PC) matrix $\mathbf{X} \in \mathbb{R}^{D \times N}$, and the mixing matrix $\mathbf{W} \in \mathbb{R}^{D \times D}$. Let $\mathbf{X}^C$ and $\mathbf{W}^C$ be the reduced PC and mixing matrices consisting of the first C rows of $\mathbf{X}$ and $\mathbf{W}$, respectively. $\mathrm{X}^C(n)$ is now MVAR-modeled, and the modeled time series $\hat{\mathrm{X}}^C(n)$ is afterwards transformed back into the original HD space via left multiplication of the pseudo inverse $\mathbf{W}^{C+}$ of $\mathbf{W}^C$. The residuals of the whole model are then gained by $\hat{\mathbf{E}} = \mathbf{W}^{C+}\hat{\mathbf{X}}^C - \mathbf{Y}$.

For the GCI procedure, information of any channel has to be canceled successively by reducing the data to $\mathbf{Y}^{d-} \in \mathbb{R}^{D-1 \times D}$, where the d-th row of $\mathbf{Y}$ is deleted. In the framework of lsGCI this can be accomplished by an enclosed modification of the reduced mixing matrix $\mathbf{W}^C$: For any d-th elimination step, $\mathbf{W}$ is reduced to $\mathbf{W}^{d-}$ by eliminating the last $D - C$ rows and the d-th column. The reduced PCA data are then gained by $\mathbf{X}^{d-} = \mathbf{W}^{d-}\mathbf{Y}^{d-}$ and the obtained model residuals can be transferred back to HD space via $\hat{\mathbf{E}}^{d-} = \mathbf{W}^{d-+} \cdot \hat{\mathbf{X}}^{d-} - \mathbf{Y}^{d-}$. The lsGCI from d_1 to d_2 is then defined by $\gamma_{d_2 \leftarrow d_1} = \ln\left(\hat{\Sigma}_{d_2}^{d_1-}/\hat{\Sigma}_{d_2}\right)$, where $\hat{\Sigma}_{d_2}^{d_1-}$ and $\hat{\Sigma}_{d_2}$ are the d_2-th diagonal entries of the covariance matrices of $\hat{\mathbf{E}}^{d_1-}$ and $\hat{\mathbf{E}}$.

B. Testing statistical significance

The null hypothesis H_0 of no directed interaction from vertex j to vertex i is equivalent to $b_{ij} = 0$. We used a Monte-Carlo-Simulation with 1000 realizations to estimate the distribution of lsGCIs under H_0. Assuming that the interaction from vertex j to vertex i, $1 \leq i \neq j \leq D$ should be tested, the AR-matrix $\mathbf{B}$ is modified by setting $b_{ij} = 0$, keeping all other parameters unchanged. Using this modified AR parameter matrix a set of time series under H_0 is generated and yields a set of lsGCIs $\gamma_{i \leftarrow j}^{H_0}$ under H_0. The analytical distribution [3] was used for the classical GCI. Statistical analyses were performed with 1% type I error.

C. Module detection and comparison of network partitions

For finding binary directed network partitions into modules or clusters of vertices, we applied the Louvain method for hierarchical community decomposition based on modularity optimization [4] (implementation used: [5]).

Module preservation in the networks identified by (ls)GCI approaches can be verified by comparing their partitions with the partition of the ground truth network on which they are based. For it we computed the ratio of correctly classified vertices (CCV) with regard to their known classification (module membership), the partition distance (PD, normalized variation of information) [6], [7] and normalized mutual information between two network partitions (MI) [7]. Complementary information to the similarity of network partitions is obtained by assessing the quality of the partitions, i.e. we additionally like to distinguish "clear-cut" from "weak" network partitions. As quality functions we applied the modularity measure (Q) [8], [9], performance (PE), [9], coverage (COV) [9] and the overall average silhouette width (OSW) [10]. For Q we selected the variant that takes into account the contributions of entire modules and not contributions of vertex pairs. PE is the fraction of vertices of the same modules that are connected by an edge and of unconnected vertices that are not assigned the same module membership. COV denotes the ratio of the number of intra-community edges to total number of edges, which equals one in an ideal partition. OSW is the average over all silhouette values, quantifying the disbalance between the average intra-module dissimilarity of each vertex and its smallest average inter-module dissimilarity.

IV. RESULTS

A. Simulated data

To evaluate the effect of the embedded dimension reduction we considered Cohen's kappa (Fig. 2) for measuring the agreement between the ground truth adjacency matrix

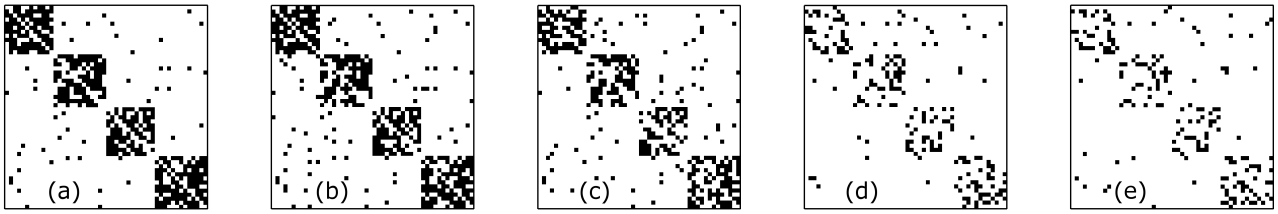

Fig. 1. Graphical representation of adjacency matrices with vertices reordered according to their module affiliation defined in the ground truth network. (a) ground truth, (b) GCI ($N = 3000$), (c) lsGCI ($N = 3000$, 40 of 50 components retained, 84% variance explanation), (d) GCI ($N = 1000$), (e) lsGCI ($N = 1000$, 40 of 50 components retained, 86% variance explanation). As expected, the preservation of adjacency information depends on time series length and degree of dimension reduction. However even though reduced, the module structure is still apparent in all cases.

(Fig. 1(a)) and adjacency matrices identified by (ls)GCI approaches. Some corresponding example adjacency matrices are shown in Fig. 1(b)-(e). In the case of the longer time series, $N = 3000$, the agreement with the ground truth is substantial up to very good. For $N = 1000$, the agreement may be considered as moderate for the GCI and lsGCIs retaining not less than 35 of 50 components, which corresponds to a variance explanation of at least 78%. For long time series, it was shown that a reduced number of retained components indeed results in an inferior correctness of lsGCI results. However, for reasonable dimension reductions the agreement is kept within acceptable limits. In contrast, for smaller numbers of samples positive effects of dimension reduction on sensitivity and specificity may be observed [2]. A second aspect is the influence of the embedded dimension reduction on the detectable module affiliation, which is demonstrated on the basis of partitions obtained by the Louvain algorithm. Partitions of networks identified by (ls)GCI approaches were compared to the known module affiliation of vertices in the ground truth network. Considering CCV, PD and the MI, the impact is manageable for $N = 1000$ (Table I). For $N = 3000$ all quantities are constant (CCV = MI = 1, PD = 0) with respect to all (ls)GCI approaches and the module structure could be fully recovered. Similarly, for $N = 1000$ and $N = 3000$ the quality of the detected modules is high as revealed by Q, PE, COV and OSW. As expected, the quality is better for $N = 3000$, although here the PE is slightly smaller (Table II). In summary, the module preservation is very good, and the influence of the dimension reduction on module recoverability and module quality is much lower than one might assume by comparing edge patterns only (Fig. 2) or comparing graphical representations of adjacency matrices (Fig. 1).

TABLE I

NETWORK PARTITIONING: VERIFICATION OF MODULE PRESERVATION

N = 1000		CCV	PD	MI
GCI		0.924	0.116	0.852
lsGCI	45/50, 93%	0.892	0.177	0.795
	40/50, 86%	0.860	0.237	0.743
	35/50, 78%	0.898	0.169	0.807
	30/50, 69%	0.873	0.209	0.765

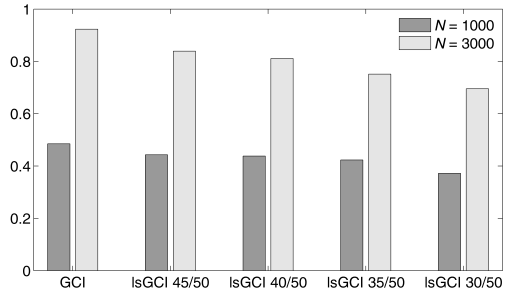

Fig. 2. Assessment of detection accuracy by Cohen's kappa. The ratios at the abscissa denote the proportion of retained components.

B. Functional resting state MRI data

The high dimensionality of the fMRI data necessitates our new large-scale GCI approach since no GCI-networks could be computed ($D > N$). Following the multiscale framework of multiple thresholding of connectivity matrices we dichotomized lsGCI-matrices at different threshold levels [11] and subsequently performed the module detection on the resulting binary networks. Similar to the simulated data set it is noticeable, that the effect of the embedded dimension reduction on the module structure seems small enough for modules to be recoverable (Fig 3). Additionally, for our pilot study data, the module structure is also more robust with respect to threshold modifications as we expected, although the network topology is directly affected. Most likely this can be attributed to the fact that intra- and inter-module connections are similarly influenced by threshold alterations. It is notable that the dimension reduction with the highest variance explanation does not necessarily result in the most pronounced segmentation, when D increases in relation to N. That effect was already described in [2] for artificial data and can be observed here again. In summary, variance explanations around 80% results in very similar module structures (Fig. 3).

V. CONCLUSIONS AND FUTURE WORK

It could be shown that an appropriate dimension reduction can be integrated into time series models for extending the GCI to HD data. As expected, the degree of dimension reduction affects the resulting identified network topology. Yet, we found only little impact on the module structure,

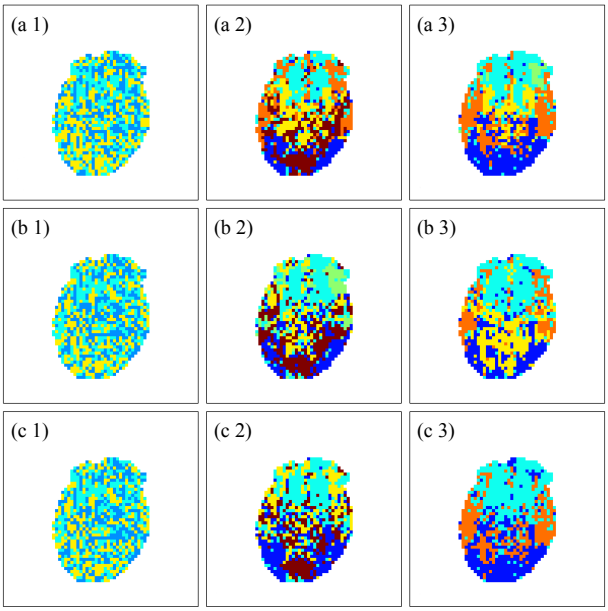

Fig. 3. Functional segmentation of identified modules for various degrees of dimension reduction and threshold levels. The columns represents modular structure of lsGCI networks with different levels of variance explanation (from left to right, 90%, 85% and 80%). The rows show segmentation in dependence on different threshold levels used for network dichotomization (a: 80%-, b: 60%- and c: 40%-percentiles of lsGCI values). For all thresholds, dichotomized networks consisted of one connected component.

TABLE II

NETWORK PARTITIONING: MODULE QUALITY ASSESSMENT

N = 1000		**Q**	**PE**	**COV**	**OSW**
ground truth		0.651	0.914	0.903	0.395
GCI		0.529	0.858	0.731	0.090
lsGCI	45/50, 93%	0.454	0.883	0.602	0.063
	40/50, 86%	0.422	0.907	0.547	0.059
	35/50, 78%	0.441	0.881	0.602	0.059
	30/50, 69%	0.438	0.894	0.575	0.049

N = 3000		**Q**	**PE**	**COV**	**OSW**
ground truth		0.651	0.914	0.903	0.395
GCI		0.593	0.895	0.845	0.332
lsGCI	45/50, 92%	0.571	0.872	0.824	0.258
	40/50, 84%	0.571	0.866	0.824	0.237
	35/50, 75%	0.591	0.858	0.844	0.218
	30/50, 66%	0.588	0.849	0.839	0.202

which is of particular interest when the detection of functional similar vertices (voxels in the case of fMRI data) is the primary objective. This result is remarkable in so far as network modules in connectivity networks might represent a map of regions with similar connectivity characteristics. Still, interpretation of module structure projected back to fMRI slices might be difficult, depending on prior physiological knowledge, definiteness and localization of modules. Segmentation of large-scale binary directed functional connectivity networks is threshold-dependent. As a first approach to deal with it, we performed an exploratory analysis of different threshold levels [11] and showed that main features of the module structure were preserved over a wide range of thresholds and levels of variance explanation. Clearly, more elaborate ways of dichotomizing weighted lsGCI networks have to be applied in the future. From the practical point of view, the determination of the optimal degree of dimension reduction is still an open question. In the case of short time series, it does not seem to be appropriate to explain as much variance as technically possible. Here, a stronger dimension reduction appears more appropriate - most likely because less AR parameters have to be estimated resulting in reduced estimator variances.

REFERENCES

[1] Roebroeck A., Formisano E., Goebel R., 2005. Mapping directed influence over the brain using Granger causality and fMRI. NeuroImage 25, 230-242.

[2] Pester, B., Leistritz, L., Witte, H., Wismueller, A., 2013. Exploring Effective Connectivity by a Granger Causality Approach with Embedded Dimension Reduction. Biomed Tech 58, 1.

[3] Gourvitch, B., Le Bouquin-Jeanns, R., Faucon, G., 2006. Linear and nonlinear causality between signals: methods, examples and neurophysiological applications. Biological Cybernetics 95, 349-369.

[4] Blondel VD, Guillaume J-L, Lambiotte R, Lefebvre E, 2008. Fast unfolding of communities in large networks. J Stat Mech 2008, P10008.

[5] Antoine Scherrer, 2014. http://perso.uclouvain.be/vincent.blondel/research/louvain.html

[6] Rubinov M, Sporns O, 2010. Complex network measures of brain connectivity: Uses and interpretations. NeuroImage 52, 1059-1069.

[7] Meila M, 2007. Comparing clusterings: an information based distance. Journal of Multivariate Analysis 98, 873-895.

[8] Leicht EA, Newman MEJ, 2008. Community structure in directed networks. Phys Rev Lett 100: 118703.

[9] Fortunato S, 2010. Community detection in graphs. Physics Reports 486, 75-174.

[10] Rousseeuw PJ, 1987. Silhouettes: A graphical aid to the interpretation and validation of cluster analysis. Journal of Computational and Applied Mathematics 20, 53-65.

[11] Lee, H., Kang, H., Chung, M.K., Kim, B.-N., Lee, D.S., 2012. Persistent Brain Network Homology From the Perspective of Dendrogram. IEEE Transactions on Medical Imaging 31(12), 2267-2277.